Droplet Differentiation by a Chemical Switch

Xi Chen,[1] Rabea Seyboldt,[2] Jens-Uwe Sommer,[1,5,6] Frank Jülicher,[2,3,4,5] and Tyler Harmon[1,*]
[1]Leibniz-Institut für Polymerforschung, Institut Theorie der Polymere, 01069 Dresden, Germany
[2]Max Planck Institute for the Physics of Complex Systems, Nöthnitzerstrasse 38, 01187 Dresden, Germany
[3]Max Planck Institute of Molecular Cell Biology and Genetics, Pfotenhauerstrasse 108, 01307 Dresden, Germany
[4]Center for Systems Biology Dresden, 01307 Dresden, Germany
[5]Cluster of Excellence Physics of Life, TU Dresden, 01062 Dresden, Germany
[6]Institute for Theoretical Physics, TU Dresden, Zellescher Weg 17, 01069 Dresden, Germany

(Received 22 September 2023; accepted 29 May 2024; published 9 July 2024)

A fundamental question about biomolecular condensates is how distinct condensates can emerge from the interplay of different components. Here we present a minimal model of droplet differentiation where phase separated droplets demix into two types with different chemical modifications triggered by enzymatic reactions. We use numerical solutions to Cahn-Hilliard equations with chemical reactions and an effective droplet model to reveal the switchlike behavior. Our work shows how condensate identities in cells could result from competing enzymatic actions.

DOI: 10.1103/PhysRevLett.133.028402

Cells organize biochemistry in space through the formation of distinct chemical compartments. Membranes provide barriers to separate different compartments. However, many compartments do not have membranes which are called biomolecular condensates because they are dense assemblies of specific types of molecules [1–6]. Biomolecular condensates are often very dynamic in that they exhibit a fast exchange of molecules with the surrounding cytoplasm and behave similar to liquid droplets [7–9]. Liquidlike properties make them well suited to act as reaction centers that concentrate specific enzymes and substrates together in a small volume, thereby localizing biochemical processes in distinct spaces [10–12].

Over the past decade, many different membraneless compartments have been identified [1,5,13–19]. These compartments typically consist of proteins and nucleic acids that coexist with their surrounding medium as a phase separated liquid mixture. A fundamental question in biology is how, from a cytoplasm with a large number of different molecular components, specific types of condensates emerge and what determines their identity. In principle, phase separation of multicomponent systems permits the coexistence of multiple different phases according to the Gibbs rule. However it is unclear how biology could control the coexistence of many different phases and how this could define the identities of condensates observed in cells. An alternative for cells is to use chemical modifications of molecules to organize the biochemical identity of compartments.

Proteins that participate in the formation of biomolecular condensates can be subjected to posttranslational modifications, including for example acetylation, methylation, and, in particular, phosphorylation [20,21]. Protein phosphorylation is carried out by enzymes called kinases, which can add one or more phosphate groups to a target protein. Those phosphate groups can be removed by another type of enzyme known as phosphatase. Changes in the phosphorylation state of condensate-associated proteins can induce the formation or the dissolution of droplets [22–25], or affect the interactions of molecules that partition into droplets [26,27].

The introduction of chemical modifications to the molecular components in a phase separating system can lead to novel nonequilibrium droplet dynamics. Here we present a minimal model to discuss droplet differentiation as an emergent feature of chemically active droplets. We show that chemical modifications can drive a single population of droplets to become unstable and split into two subpopulations of differentiated droplets, whereby the same underlying physical interactions drive phase separation, yet condensate constituents from the two droplets have different chemical identities. These differentiated droplets have different chemical properties and in a cell could provide different functions.

We consider the simple case where the chemical modifications do not affect the thermodynamics of phase separation, but change the partitioning of enzymes into the droplets. Our model system consists of five components. Solvent W in a biological system is water based. Droplet material phase separates from the solvent. This material, which we call scaffold, exists in two chemical states, A and B. We consider that A and B have the same interactions with solvent W, which corresponds to the case where posttranslational modifications of one monomer have only a small effect on the thermodynamics of phase separation. Two enzymes denoted AB and BA convert scaffold state A to B and B to A, respectively, through the reactions

$$A + AB \rightarrow B + AB, \tag{1}$$

$$B + BA \rightarrow A + BA, \tag{2}$$

shown schematically in Fig. 1(b). The modification A to B is motivated by phosphorylation of proteins in a cell, which requires an energy input that is not described explicitly, and therefore the rates of the reaction do not obey detailed balance. The enzymatic reactions are described by Michaelis-Menten kinetics, giving a net chemical reaction flux of component A as

$$Y = -k_{AB}\frac{n_{AB}n_A}{K_{AB}+n_A} + k_{BA}\frac{n_{BA}n_B}{K_{BA}+n_B}, \tag{3}$$

where the first term corresponds to reaction (1) and the second term corresponds to reaction (2), n_i is the concentration of component i, k_{AB} and k_{BA} are kinetic coefficients that describe the enzyme speed, and K_{AB} and K_{BA} characterize the strength of binding of enzymes with their substrates.

The key aspect of the model is that the enzymes have a preference to partition into droplets that are composed of the product of the respective enzymes' reaction; see Fig. 1(c). Such a situation could arise for example if the enzyme possessed two domains, a catalytic (kinase) domain, and a binding domain that bound the phosphorylated target protein.

We describe the system by the free energy [28]

$$F = \int dV\left[f + \frac{\kappa}{2}(\nabla n_W)^2\right]. \tag{4}$$

The integration is over the system volume in three dimensions (3D) or area in two dimensions (2D), the gradient term with strength κ captures an emergent surface tension, and f is the free energy density, which primarily controls the bulk properties. We use a Flory-Huggins free energy density of the form [29,30]

$$\frac{f}{k_BT} = -\chi v(n_A+n_B+n_{BA}+n_{AB})^2 - \varepsilon v(n_A-n_B)(n_{BA}-n_{AB}) + \sum_i n_i \log n_i v_i. \tag{5}$$

Here χ describes the interaction enabling phase separation of scaffolds and enzymes from the solvent, and ε describes the interaction that promotes the enzymes to colocalize with their products. The logarithm terms capture the entropy of mixing, and v_i is the molecular volume of component i where the sum runs over all components including solvent $i = \{W, A, B, AB, BA\}$. Furthermore, we consider an incompressible system with constant molecular volumes v_i such that concentrations obey the constraint $\sum_i n_i v_i = 1$. In the following we use parameters for which the system has two coexisting phases, a droplet phase and a bulk phase.

To focus on the core features of this model, we choose for simplicity symmetric parameters: equal molecular volumes for all solute species $v_i = v$, equal enzyme rate coefficients $k = k_{AB} = k_{BA}$, and enzyme association constants $K = K_{AB} = K_{BA}$. As initial conditions we choose equal average concentrations $\bar{n}_A = \bar{n}_B$ and $\bar{n}_{AB} = \bar{n}_{BA}$.

Our model can be related to biomolecular condensates where the scaffold in modification state A and B is a single class of proteins that can condense to form droplets. The two enzymes AB and BA convert the protein between two states, such as phosphorylated and unphosphorylated states. The idea that enzymes tend to colocalize with their reaction products, as described by the coefficient ε, could for example correspond to kinases with two domains as in Fig. 1(c); see also the Supplemental Material [31]. This biases the enzymes to be localized with their products. As we show below, droplets that are enriched toward one of the modification states tend to recruit enzymes that further modify the droplet in the same direction. This is a positive feedback that can cause the droplets to diverge into differentiated droplets.

We first discuss the dynamics of the system using Cahn-Hilliard equations with added reaction terms [28]:

$$\partial_t n_A = \Gamma\nabla^2\mu_A + Y, \tag{6}$$

$$\partial_t n_B = \Gamma\nabla^2\mu_B - Y, \tag{7}$$

$$\partial_t n_{AB} = \Gamma\nabla^2\mu_{AB}, \tag{8}$$

$$\partial_t n_{BA} = \Gamma\nabla^2\mu_{BA}. \tag{9}$$

Here, Γ is the mobility coefficient of the components and $\mu_i = \delta F/\delta n_i$ denotes the exchange chemical potential of component i. For 3D systems, when not otherwise noted, we use interaction parameter $\chi = 2.5$, molecular volumes $v = v_W = 10^2$ nm^3, initial average scaffold concentration $\bar{n}_s = 3\times10^{-3}$ nm^{-3}, and $\kappa = 2\times10^6\ k_BT$nm^5. These

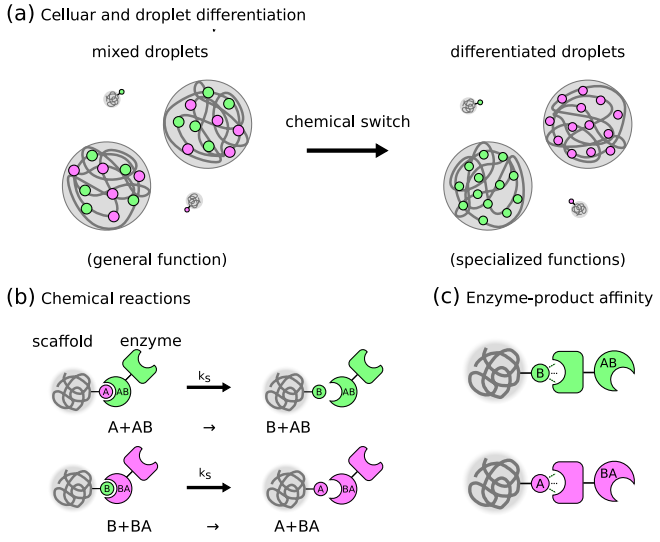

FIG. 1. Cartoon representation of our system. (a) Droplets differentiate to acquire new unique volumes (mixed to green and magenta droplets). (b) Scaffold protein is modified between two states, A and B, by two enzymes AB and BA. (c) Enzymes associate with their products through nonreactive domains.

values ensure that the system is located in the two-phase region of the phase diagram. We also use a mobility coefficient $\Gamma = 2 \times 10^4\ k_B^{-1}T^{-1}\,\mathrm{nm}^{-1}\,\mathrm{s}^{-1}$, which corresponds to a dilute phase diffusion coefficient for scaffold around 20 $\mu\mathrm{m}^2/\mathrm{s}$, initial ratio of average scaffold concentration to enzyme concentration $\bar{n}_s/\bar{n}_e = 10$, and $K = 10^{-4}\ \mathrm{nm}^{-3}$. These values are motivated by relatively low enzyme concentrations and strong enzyme-substrate binding; see the Supplemental Material [31]. For 2D systems, when not otherwise noted, we use $v = v_W = 10^2\ \mathrm{nm}^2$, $\bar{n}_s = 3 \times 10^{-3}\ \mathrm{nm}^{-2}$, $\kappa = 2 \times 10^6\ k_BT\,\mathrm{nm}^4$, $\Gamma = 2 \times 10^4\ k_B^{-1}T^{-1}\ \mathrm{s}^{-1}$, and $K = 10^{-4}\ \mathrm{nm}^{-2}$. We solve the resulting dynamic equations numerically using a Fourier spectral method combined with an implicit-explicit method [35]; see the Supplemental Material [31].

We start by considering two identical droplets in 2D space containing equal amounts $n_A = n_B$ of scaffold and $n_{AB} = n_{BA}$ of enzyme concentrations with a small superimposed random variation in concentration. We find that the droplets differentiate spontaneously as time proceeds: one droplet enriches A, while the second (partner) droplet enriches B, as shown in Fig. 2(a). Enzymes similarly partition into the two droplets following their products. When we turn off the chemical reactions, the droplets recover the state where A and B are mixed in both droplets, showing that the differentiation of the droplets is reversible. Solving the dynamic equations in 3D, we find qualitatively the same behavior as in 2D; see Fig. 2(c).

We also study the case where there are no nearby droplets to exchange material with, a system with the same average concentration of all the components as above but has a single droplet. This droplet quickly becomes polarized; one half enriches A, and the other half enriches B, as shown in Fig. 2(d). Additionally, the droplet proceeds to deform, divide, and separate into two differentiated droplets of different composition. Interestingly, these droplets are repulsive even though surface tension favors droplet fusion; see the Supplemental Material [31].

We describe the system in terms of the total concentrations $n_{e,s}$, and the excess concentrations $\delta_{e,s}$ with

$$n_e = n_{BA} + n_{AB}, \qquad \delta_e = n_{BA} - n_{AB},$$
$$n_s = n_A + n_B, \qquad \delta_s = n_A - n_B. \tag{10}$$

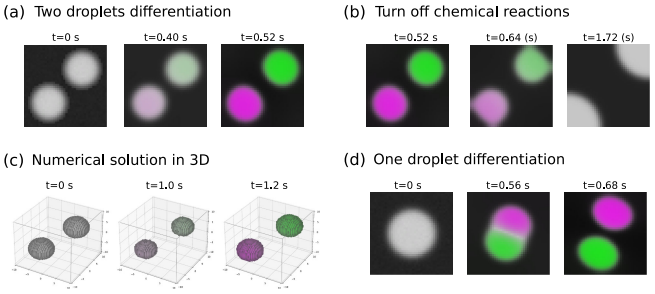

FIG. 2. Numerical solutions of reaction-diffusion Cahn-Hilliard equations of droplet differentiation. Brightness shows the total concentration of scaffolds n_s, and the color (magenta/green) shows the relative abundance of one scaffold over the other, δ_s. Note that the enzymes follow the scaffolds behavior see the Supplemental Material [31]. (a) Differentiation of two droplets in 2D. (b) Differentiation decays when the chemical reactions are turned off. (c) Differentiation in 3D. (d) Solution of a single droplet which differentiates and divides. No-flux boundary conditions were used, see the Supplemental Material [31] for periodic boundary conditions. The parameters are $\chi = 2.5$, $\varepsilon = 1.2$, $\Gamma = 2\times10^4\ k_B^{-1}T^{-1}\,\mathrm{nm}^{-1}\,\mathrm{s}^{-1}$, $\kappa = 2 \times 10^6\ \mathrm{nm}^4$, $\bar{n}_s = 3 \times 10^{-3}\ \mathrm{nm}^{-2}$, $v = 10^2\ \mathrm{nm}^2$, $K = 10^{-4}\ \mathrm{nm}^{-2}$, and $k = 250\ \mathrm{s}^{-1}$ in (a), (c), and (d), and $k = 0\ \mathrm{s}^{-1}$ in (b). The average scaffold concentrations are $\bar{n}_s = 1.8 \times 10^{-3}\ \mathrm{nm}^{-3}$ in 3D solutions.

We note that $\delta_{e,s}$ can be interpreted as an order parameter of droplet differentiation: zero values of δ indicate an undifferentiated state.

To obtain a general idea of how this system behaves, we first study droplet differentiation using an effective droplet model, a reaction-diffusion model with a sharp droplet interface [9,42]. This approximation allows an analytical solution to determine the differentiation transition as a function of the system parameters. We consider two droplets of equal size coexisting with a dilute phase. The concentration of all the components is considered homogeneous inside the droplets. We consider one droplet with composition inside described by variables $n^-_{e,s}$ and $\delta^-_{e,s}$. By symmetry the composition inside the second droplet is given by the same $n^-_{e,s}$ and by $-\delta^-_{e,s}$. The dilute phase concentrations outside both droplets are denoted by $n^+_{e,s}$ and $\delta^+_{e,s}$.

The dynamic equations from the effective droplet model for the droplet considered above are (see the Supplemental Material [31])

$$\partial_t \delta_e^- = -\frac{3D_e^+ n_s^+}{2R^2 n_s^-}\left((n_e^- + \delta_e^-)\exp(-\varepsilon v \delta_s^-) - (n_e^- - \delta_e^-)\exp(\varepsilon v \delta_s^-)\right),$$
$$\partial_t \delta_s^- = -\frac{3D_s^+ n_s^+}{R^2 n_s^-}\delta_s^- + 2k\frac{(n_e^- n_s^- - \delta_e^-\delta_s^-)\delta_s^- + (n_s^-\delta_e^- - n_e^-\delta_s^-)(2K + n_s^-)}{(2K + n_s^-)^2 - \delta_s^{-2}}, \tag{11}$$

where D_e^+ and D_s^+ are the diffusion coefficients outside the droplet for the enzymes and scaffolds, and R is the radius of the droplets. The total concentrations $n_e^\pm$ and $n_s^\pm$ are the result of the phase separation physics determined by the parameters χ and v_i and are time independent in this case. The nullclines of the dynamics are defined by the conditions $\partial_t \delta^-_{e,s} = 0$ shown as lines in the (δ_e^-, δ_s^-) plane; see Fig. 3. The intersecting points of the nullcline represent stationary

states. For small values of k there is a single stationary point where the nullclines intersect at the droplet state $(\delta_e^-, \delta_s^-) = 0$, which is stable; see Fig. 3(a). In this state droplets are mixtures of A and B. For large values of k, this stationary point becomes unstable and two stable stationary points emerge, corresponding to the two differentiated states where droplets are either enriched in A or B; see Fig. 3(b).

Using a linear stability analysis, we obtain the conditions when mixed droplets are unstable. The linearized dynamics read as

$$\begin{bmatrix} \partial_t \delta_e^- \\ \partial_t \delta_s^- \end{bmatrix} = \begin{bmatrix} -3\frac{D_e^+ n_s^+}{R^2 n_s^-} & 3\frac{D_e^+ n_s^+}{R^2 n_s^-}\varepsilon v n_e^- \\ \frac{2kn_s^-}{2K+n_s^-} & -3\frac{D_s^+ n_s^+}{R^2 n_s^-} - 4\frac{kn_e^- K}{(2K+n_s^-)^2} \end{bmatrix} \begin{bmatrix} \delta_e^- \\ \delta_s^- \end{bmatrix}, \quad (12)$$

which corresponds to exponentially varying time dependence $(\delta_e^-, \delta_s^-) \sim e^{\lambda t}$. The linear problem has two eigenvalues:

$$\lambda^{\pm} = -\frac{3n_s^+(D_s^+ + D_e^+)}{2R^2 n_s^-} - \frac{2kn_e^- K}{(2K+n_s^-)^2} \pm \sqrt{\left(\frac{3n_s^+(D_s^+ - D_e^+)}{2R^2 n_s^-} + \frac{2kn_e^- K}{(2K+n_s^-)^2}\right)^2 + \frac{6kn_e^- D_e^+ \varepsilon v n_s^+}{R^2(2K+n_s^-)}}. \quad (13)$$

The smaller eigenvalue λ^- is always negative describing stable dynamics. The larger eigenvalue λ^+ is positive when

$$-\frac{3D_s^+ n_s^+}{R^2 n_s^-} - \frac{4kKn_e^-}{(2K+n_s^-)^2} + \frac{2\varepsilon v k n_e^- n_s^-}{2K+n_s^-} > 0. \quad (14)$$

Here, the first term is the diffusion rate of the scaffolds, and the second term describes the backward chemical reaction rate. Both drive the system toward the mixed state. The third term describes the rate of the enhanced chemical reaction resulted from the localization of enzymes with their products, which destabilizes the system and induces differentiation. When the last term dominates the system, λ^+ becomes positive, and the system will spontaneously differentiate into two different subpopulations of droplets; see Fig. 3(c).

Figure 3(d) shows the state diagram in the (ε, k) plane for fixed K, R and initial average concentrations. A critical line describes the transition from a symmetric, undifferentiated state to a differentiated state. Above this line, droplets will differentiate, and below droplets stay mixed. Equation (14) matches quantitatively with the numerical results, showing that the analytical expression predicts the differentiation transition as a function of the system parameters.

The dynamics of droplet differentiation are quite rich depending on the number of droplets and extent of ripening. We return to our numerical solutions of the Cahn-Hilliard description to map out the most prevalent features; see Fig. 4(a). As discussed above, for small values of ε and k (tan region), droplets do not differentiate. For medium ε and k values (blue region), droplets do differentiate.

The instability associated with droplet differentiation is facilitated when there is a partner droplet in the system with which material can be exchanged as revealed by the region where two droplets will differentiate but one droplet stays mixed (light blue region). However, when moving in the medium blue region, single droplets also differentiate and split, showing that droplet differentiation is robust and does not require material exchange with other droplets. For even higher values of ε and k (dark blue region), droplets polarize into multiple domains before they divide into many droplets. The resulting droplets undergo ripening and coalescence until there are exactly two differentiated droplets of the same size; see the Supplemental Material [31], Sec. VIII, for systems starting with many droplets.

We can compare this ripening to Ostwald ripening [43], the thermodynamic process where small droplets shrink and big droplets grow until there is only one droplet.

First we study the ripening of the same type of differentiated droplets; we consider a system of four droplets, two big droplets and two small droplets; see Fig. 4(b). As shown in the snapshots, small droplets in the differentiated system dissolve faster than the undifferentiated system. Differentiation thus enhances Ostwald ripening kinetics between droplets of the same type. Next we investigate the ripening of opposite types of droplets; we consider a system with a big droplet of A and a small droplet of B; see Fig. 4(c). The two differentiated droplets equalize to the same size, indicating that material is transported from the big droplet to the small droplet. Differentiation thus reverses Ostwald ripening kinetics between droplets of opposite type. Taken together, differentiated droplet systems rapidly converge to two equalized droplets instead of slowly reaching the expected final state of one droplet.

Our work shows that phase separation together with protein modification can generate a biochemical switch that can provide different identities to biomolecular condensates via droplet differentiation. Differentiated droplets recruit different enzymes and contain different modifications to the scaffold. The prerequisite is droplets with competing enzymes having preferential affinity for their own products. The switchlike behavior of droplet differentiation could enable droplets formed by a single type of interaction that drives phase separation to be specialized for different functions. An important feature of this differentiation is that it can be regulated by external signals such as enzyme activation and deactivation to convert the droplets between differentiated (specialized) and undifferentiated (general) states.

Labeled scaffold proteins are often used to identify the location and type of biological condensates as foci that reveal the presence of dense assemblies of scaffold [12]. As we show in our work, droplet differentiation implies that droplets can have different biochemical identities even though the scaffold is the same. Therefore a careful analysis including protein modifications may be required to fully identify condensates in cells and to distinguish differentiated droplets.

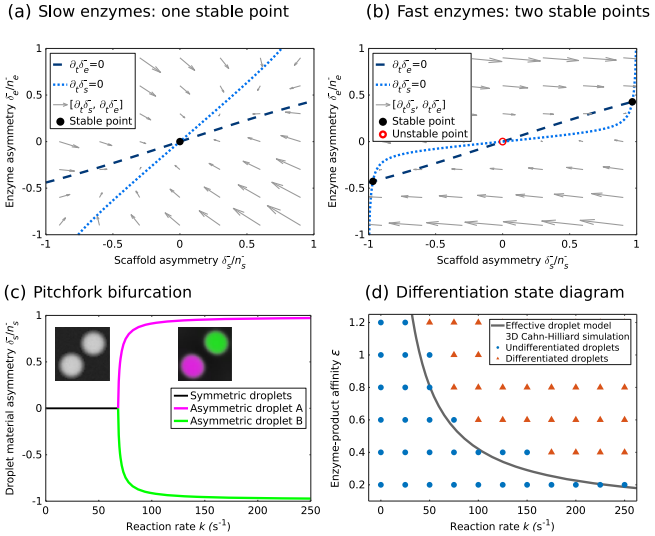

FIG. 3. Droplet differentiation in effective droplet model. (a),(b) Vector maps of the time dependency for the asymmetry of scaffolds δ_s and asymmetry of enzymes δ_e with (a) low reaction rate, $k = 25\ \mathrm{s}^{-1}$ and (b) fast reaction rate, $k = 250\ \mathrm{s}^{-1}$. The arrow vector shows $(\partial_t\delta_s^-, \partial_t\delta_e^-)$. The lines are the nullclines where $\partial_t\delta_e^- = 0$ (dashed) and $\partial_t\delta_s^- = 0$ (dotted). The system has stationary points where the two lines intersect. The stable stationary points are denoted with a black dot. For a low reaction rate there is only one stationary point at $\delta^- = 0$. For a fast reaction rate there are two stationary points corresponding to differentiated droplets. (c) Stable stationary points as a function of enzyme reaction rate k. At a critical enzyme speed the system undergoes a pitchfork bifurcation into two different types of droplets. (d) State diagram in the (ε, k) plane. The symbols are 3D numerical results, and the line is the analytical results from the effective droplet model. The parameters are $n_s^+ = 1.4 \times 10^{-3}\ \mathrm{nm}^{-2}$, $n_s^- = 7.9 \times 10^{-3}\ \mathrm{nm}^{-2}$, $n_e^- = 7.9 \times 10^{-4}\ \mathrm{nm}^{-2}$, $v = 10^2\ \mathrm{nm}^2$, $D_e^+ = 281\ \mu\mathrm{m}^2\ \mathrm{s}^{-1}$, $D_s^+ = 28.1\ \mu\mathrm{m}^2\ \mathrm{s}^{-1}$, $R = 1.6\ \mu\mathrm{m}$, and except for (d), $\varepsilon = 0.6$.

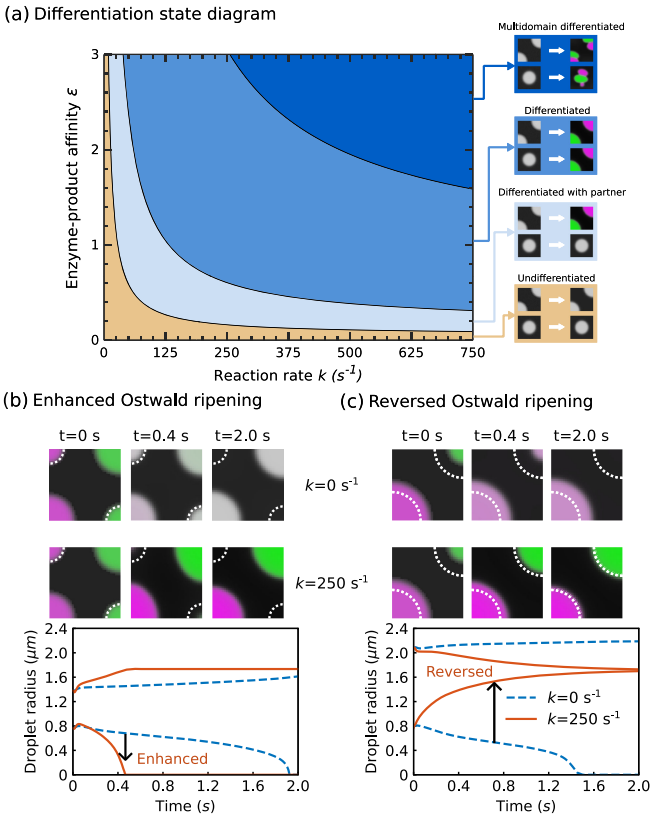

FIG. 4. (a) Differentiation state diagram of droplet differentiation in 2D. In the plane of ε, k are four regimes corresponding to undifferentiated (tan), differentiated with partner(light blue), differentiated (medium blue), and multidomain differentiated (dark blue) areas. The snapshots from solutions in different parameter regimes are shown in the legend. (b) The enhanced ripening between the same type of droplets. (c) The reversed ripening between different types of droplets. Dotted lines in snapshots are visualization aids to highlight the ripening. Line plots show the radii change over time of the big and small droplets. The arrows highlight the impact from the droplet differentiation. No-flux boundary conditions were used. The parameters are $\chi = 2.5$, $\Gamma = 2 \times 10^4\ k_B^{-1}T^{-1}\ \mathrm{nm}^{-1}\ \mathrm{s}^{-1}$, $\kappa = 2 \times 10^6\ \mathrm{nm}^4$, $\bar{n}_s = 3 \times 10^{-3}\ \mathrm{nm}^{-2}$, $v = 10^2\ \mathrm{nm}^2$, and $K = 10^{-4}\ \mathrm{nm}^{-2}$. The ripening calculations used $\varepsilon = 0.5$.

We also showed that droplet differentiation can induce droplet polarization and division into multiple droplets. Previous work has shown that the addition of chemical reactions can either enhance [44] or reverse Ostwald ripening [16,45]. Interestingly, differentiated droplets can both enhance and reverse Ostwald ripening kinetics at the same time.

We note that coupling droplet differentiation with surface interactions or taking into account geometric restrictions such as small pores or cavities can be an interesting subject for future studies.

We note two observations that support that living cells have the needed building blocks in place for droplet differentiation. First, kinases have long been known to have nonenzymatic binding sites for their products [46–48]. Second, scaffold proteins in droplets have been shown to recruit different molecules depending on their posttranslational modifications [23,27]. In order to illustrate how our concept of droplet differentiation can be realized with proteins, we propose a possible design of multidomain proteins involving a scaffold protein, kinase, and phosphatase to interact as described in the model; see the Supplemental Material [31] for protein sequences. Our theoretical work could be tested in in-vitro experiments on protein condensates. It also provides a physical mechanism for the generation of condensates of different identities in cells.

We would like to thank Anthony A. Hyman, Jie Wang, Martine Ruer, and Regis Lemaitre for useful discussions about this project.

*tylerharmon@ipfdd.de

[1] C. P. Brangwynne, C. R. Eckmann, D. S. Courson, A. Rybarska, C. Hoege, J. Gharakhani, F. Jülicher, and

A. A. Hyman, Germline p granules are liquid droplets that localize by controlled dissolution/condensation, Science **324**, 1729 (2009).
[2] P. Li, S. Banjade, H.-C. Cheng, S. Kim, B. Chen, L. Guo, M. Llaguno, J. V. Hollingsworth, D. S. King, S. F. Banani, P. S. Russo, Q.-X. Jiang, B. T. Nixon, and M. K. Rosen, Phase transitions in the assembly of multivalent signalling proteins, Nature (London) **483**, 336 (2012).
[3] A. A. Hyman, C. A. Weber, and F. Jülicher, Liquid-liquid phase separation in biology, Annu. Rev. Cell Develop. Biol. **30**, 39 (2014).
[4] A. Patel, H. Lee, L. Jawerth, S. Maharana, M. Jahnel, M. Hein, S. Stoynov, J. Mahamid, S. Saha, T. Franzmann, A. Pozniakovski, I. Poser, N. Maghelli, L. Royer, M. Weigert, E. Myers, S. Grill, D. Drechsel, A. Hyman, and S. Alberti, A liquid-to-solid phase transition of the als protein fus accelerated by disease mutation, Cell **162**, 1066 (2015).
[5] S. F. Banani, H. O. Lee, A. A. Hyman, and M. K. Rosen, Biomolecular condensates: Organizers of cellular biochemistry, Nat. Rev. Mol. Cell Biol. **18**, 285 (2017).
[6] T. Mittag and R. V. Pappu, A conceptual framework for understanding phase separation and addressing open questions and challenges, Mol. Cell **82**, 2201 (2022).
[7] M. Dundr, M. D. Hebert, T. S. Karpova, D. Stanek, H. Xu, K. B. Shpargel, U. T. Meier, K. M. Neugebauer, A. G. Matera, and T. Misteli, In vivo kinetics of cajal body components, J. Cell Biol. **164**, 831 (2004).
[8] S. Weidtkamp-Peters, T. Lenser, D. Negorev, N. Gerstner, T. G. Hofmann, G. Schwanitz, C. Hoischen, G. Maul, P. Dittrich, and P. Hemmerich, Dynamics of component exchange at PML nuclear bodies, J. Cell Sci. **121**, 2731 (2008).
[9] C. A. Weber, D. Zwicker, F. Jülicher, and C. F. Lee, Physics of active emulsions, Rep. Prog. Phys. **82**, 064601 (2019).
[10] M. Du and Z. J. Chen, DNA-induced liquid phase condensation of cGAS activates innate immune signaling, Science **361**, 704 (2018).
[11] J. Sheu-Gruttadauria and I. J. MacRae, Phase transitions in the assembly and function of human mirisc, Cell **173**, 946 (2018).
[12] A. S. Lyon, W. B. Peeples, and M. K. Rosen, A framework for understanding the functions of biomolecular condensates across scales, Nat. Rev. Mol. Cell Biol. **22**, 215 (2021).
[13] S. Saha, C. A. Weber, M. Nousch, O. Adame-Arana, C. Hoege, M. Y. Hein, E. Osborne-Nishimura, J. Mahamid, M. Jahnel, L. Jawerth, A. Pozniakovski, C. R. Eckmann, F. Jülicher, and A. A. Hyman, Polar positioning of phase-separated liquid compartments in cells regulated by an mRNA competition mechanism, Cell **166**, 1572 (2016).
[14] M. Boehning, C. Dugast-Darzacq, M. Rankovic, A. S. Hansen, T. Yu, H. Marie-Nelly, D. T. McSwiggen, G. Kokic, G. M. Dailey, P. Cramer, X. Darzacq, and M. Zweckstetter, RNA polymerase II clustering through carboxy-terminal domain phase separation, Nat. Struct. Mol. Biol. **25**, 833 (2018).
[15] H. Lu, D. Yu, A. S. Hansen, S. Ganguly, R. Liu, A. Heckert, X. Darzacq, and Q. Zhou, Phase-separation mechanism for c-terminal hyperphosphorylation of RNA polymerase II, Nature (London) **558**, 318 (2018).
[16] D. Zwicker, M. Decker, S. Jaensch, A. A. Hyman, and F. Jülicher, Centrosomes are autocatalytic droplets of pericentriolar material organized by centrioles, Proc. Natl. Acad. Sci. U.S.A. **111**, E2636 (2014).
[17] J. B. Woodruff, B. Ferreira Gomes, P. O. Widlund, J. Mahamid, A. Honigmann, and A. A. Hyman, The centrosome is a selective condensate that nucleates microtubules by concentrating tubulin, Cell **169**, 1066 (2017).
[18] Y. S. Mao, B. Zhang, and D. L. Spector, Biogenesis and function of nuclear bodies, Trends Genet. **27**, 295 (2011).
[19] H. Wu, Higher-order assemblies in a new paradigm of signal transduction, Cell **153**, 287 (2013).
[20] I. Owen and F. Shewmaker, The role of post-translational modifications in the phase transitions of intrinsically disordered proteins, Int. J. Mol. Sci. **20** (2019).
[21] W. T. Snead and A. S. Gladfelter, The control centers of biomolecular phase separation: How membrane surfaces, PTMs, and active processes regulate condensation, Mol. Cell **76**, 295 (2019).
[22] Z. Monahan, V. H. Ryan, A. M. Janke, K. A. Burke, S. N. Rhoads, G. H. Zerze, R. O'Meally, G. L. Dignon, A. E. Conicella, W. Zheng, R. B. Best, R. N. Cole, J. Mittal, F. Shewmaker, and N. L. Fawzi, Phosphorylation of the FUS low-complexity domain disrupts phase separation, aggregation, and toxicity, EMBO J. **36**, 2951 (2017),.
[23] T. H. Kim, B. Tsang, R. M. Vernon, N. Sonenberg, L. E. Kay, and J. D. Forman-Kay, Phospho-dependent phase separation of FMRP and CAPRIN1 recapitulates regulation of translation and deadenylation, Science **365**, 825 (2019).
[24] A. G. Larson, D. Elnatan, M. M. Keenen, M. J. Trnka, J. B. Johnston, A. L. Burlingame, D. A. Agard, S. Redding, and G. J. Narlikar, Liquid droplet formation by HP1α suggests a role for phase separation in heterochromatin, Nature (London) **547**, 236 (2017).
[25] A. K. Rai, J.-X. Chen, M. Selbach, and L. Pelkmans, Kinase-controlled phase transition of membraneless organelles in mitosis, Nature (London) **559**, 211 (2018).
[26] S. Sridharan, A. Hernandez-Armendariz, N. Kurzawa, C. M. Potel, D. Memon, P. Beltrao, M. Bantscheff, W. Huber, S. Cuylen-Haering, and M. M. Savitski, Systematic discovery of biomolecular condensate-specific protein phosphorylation, Nat. Chem. Biol. **18**, 1104 (2022).
[27] Y. E. Guo, J. C. Manteiga, J. E. Henninger, B. R. Sabari, A. Dall'Agnese, N. M. Hannett, J.-H. Spille, L. K. Afeyan, A. V. Zamudio, K. Shrinivas, B. J. Abraham, A. Boija, T.-M. Decker, J. K. Rimel, C. B. Fant, T. I. Lee, I. I. Cisse, P. A. Sharp, D. J. Taatjes, and R. A. Young, Pol II phosphorylation regulates a switch between transcriptional and splicing condensates, Nature (London) **572**, 543 (2019).
[28] J. W. Cahn and J. E. Hilliard, Free energy of a nonuniform system. I. Interfacial free energy, J. Chem. Phys. **28**, 258 (1958).
[29] P. J. Flory, Thermodynamics of high polymer solutions, J. Chem. Phys. **10**, 51 (1942).
[30] M. L. Huggins, Theory of solutions of high polymers, J. Am. Chem. Soc. **64**, 1712 (1942).
[31] See Supplemental Material at http://link.aps.org/supplemental/10.1103/PhysRevLett.133.028402 for additional information about experimental schemes that could test droplet differentiation, relevant analytical derivations,

more detailed discussions of the numerical results, and video captions for the differentiation process, which includes Refs. [32–41].

[32] T. Kesti, A. Ruppelt, J.-H. Wang, M. Liss, R. Wagner, K. Taskèn, and K. Saksela, Reciprocal regulation of SH_3 and SH_2 domain binding via tyrosine phosphorylation of a common site in $CD_3\varepsilon^1$, J. Immunol. **179**, 878 (2007).

[33] N. Kurochkina and U. Guha, SH_3 domains: Modules of protein-protein interactions, Biophys. Rev. Lett. **5**, 29 (2013).

[34] J. Wang, J.-M. Choi, A. S. Holehouse, H. O. Lee, X. Zhang, M. Jahnel, S. Maharana, R. Lemaitre, A. Pozniakovsky, D. Drechsel, I. Poser, R. V. Pappu, S. Alberti, and A. A. Hyman, A molecular grammar governing the driving forces for phase separation of prion-like RNA binding proteins, Cell **174**, 688 (2018).

[35] U. M. Ascher, S. J. Ruuth, and R. J. Spiteri, Implicit-explicit Runge-Kutta methods for time-dependent partial differential equations, Appl. Numer. Math. **25**, 151 (1997).

[36] H. P. Erickson, Size and shape of protein molecules at the nanometer level determined by sedimentation, gel filtration, and electron microscopy, Biol. Proced. Online **11**, 32 (2009).

[37] W. Xing, D. Muhlrad, R. Parker, and M. K. Rosen, A quantitative inventory of yeast p body proteins reveals principles of composition and specificity, eLife **9**, e56525 (2020).

[38] L. Hubatsch, L. M. Jawerth, C. Love, J. Bauermann, T. Y. D. Tang, S. Bo, A. A. Hyman, and C. A. Weber, Quantitative theory for the diffusive dynamics of liquid condensates, eLife **10**, e68620 (2021).

[39] D. Davidi, E. Noor, W. Liebermeister, A. Bar-Even, A. Flamholz, K. Tummler, U. Barenholz, M. Goldenfeld, T. Shlomi, and R. Milo, Global characterization of *in vivo* enzyme catalytic rates and their correspondence to *in vitro* kcat measurements, Proc. Natl. Acad. Sci. U.S.A. **113**, 3401 (2016).

[40] A. Bar-Even, E. Noor, Y. Savir, W. Liebermeister, D. Davidi, D. S. Tawfik, and R. Milo, The moderately efficient enzyme: Evolutionary and physicochemical trends shaping enzyme parameters, Biochemistry **50**, 4402 (2011).

[41] D. Zwicker, PY-PDE: A PYTHON package for solving partial differential equations, J. Open Source Software **5**, 2158 (2020).

[42] D. Zwicker, R. Seyboldt, C. A. Weber, A. A. Hyman, and F. Jülicher, Growth and division of active droplets provides a model for protocells, Nat. Phys. **13**, 408 (2017).

[43] W. Ostwald, Studien über die bildung und umwandlung fester körper, Z. Phys. Chem. **22U**, 289 (1897).

[44] M. Tena-Solsona, J. Janssen, C. Wanzke, F. Schnitter, H. Park, B. Rieß, J. M. Gibbs, C. A. Weber, and J. Boekhoven, Accelerated ripening in chemically fueled emulsions, Chem. Syst. Chem. **3**, e2000034 (2021).

[45] D. Zwicker, A. A. Hyman, and F. Jülicher, Suppression of Ostwald ripening in active emulsions, Phys. Rev. E **92**, 012317 (2015).

[46] P. Filippakopoulos, S. Müller, and S. Knapp, SH_2 domains: Modulators of nonreceptor tyrosine kinase activity, Catal. Regul. Proteins **19**, 643 (2009).

[47] Z. Tatárová, J. Brábek, D. Rösel, and M. Novotný, SH_3 domain tyrosine phosphorylation—sites, role and evolution, PLoS One **7**, e36310 (2012).

[48] M. J. Wagner, M. M. Stacey, B. A. Liu, and T. Pawson, Molecular mechanisms of SH_2-and PTB-domain-containing proteins in receptor tyrosine kinase signaling, Cold Spring Harbor Perspect. Biol. **5**, a008987 (2013).